# Catalytic Role of Lattice Defects in the Photoassisted Oxidation of Water at (001) n-TiO2 Rutile

**ARTICLE** *in* THE JOURNAL OF PHYSICAL CHEMISTRY · JANUARY 1992



**3 AUTHORS**, INCLUDING:

Francisco Munoz
University of the Balearic Islands
**229** PUBLICATIONS **1,269** CITATIONS

# Catalytic Role of Lattice Defects in the Photoassisted Oxidation of Water at (001) n-$TiO_2$ Rutile

**P. Salvador,* M. L. García González,**

*Instituto de Química Física "Rocasolano", CSIC, Serrano 119, 28006 Madrid, Spain*

**and F. Muñoz**

*Departamento Química, Facultad de Ciencias Universidad de las Islas Baleares, 07071 Palma de Mallorca, Spain* *(Received: February 10, 1992; In Final Form: September 9, 1992)*

We report experimental data on the photocurrent–time dependence observed during the photoassisted oxidation of water at a $H_2$ reduced (001) $TiO_2$ rutile single crystal, as a function of the concentration of generated donor centers. The observed photocurrent transients are fitted with a kinetic model previously proposed, according to which the photocurrent time decay at high band-bending is controlled by the second-order rate constant, $k_2$, for $H_2O_2$ generation from the recombination of surface-bound $OH^\circ_s$ radicals, photogenerated by hole trapping at Ti-coordinated $OH^-$ ions of basic character. $k_2$ is found to increase linearly with the concentration of donor centers, $N_D$, in the range $(1.5 - 43) \times 10^{17}$ cm$^{-3}$, from $7.0 \times 10^{-15}$ to $8.5 \times 10^{-14}$ cm$^2$ s$^{-1}$. The apparent increase of the catalytic activity of $TiO_2$ surface in the photooxidation of $H_2O$ to $H_2O_2$ is attributed to the formation of $Ti_2O_3$ corundum type lattice defects during $TiO_2$ reduction process in $H_2$. The catalytic properties of these defects are thought to be associated with the short distance between $Ti^{3+}$ pairs, which makes easy covalent bonding between adsorbed $OH^\circ_s$ radicals. The $k_2$ rate constant at corundum catalytic units is estimated to be about 5 orders of magnitude greater than that corresponding to nondefective $TiO_2$ rutile areas (i.e., $\approx 5 \times 10^{-10}$ vs $\approx 5 \times 10^{-15}$ cm$^2$ s$^{-1}$).

## Introduction

Optically induced photocurrent transients have been proved to provide important kinetic information about photoreactions in photoelectrochemical cells (PEC).[1] Recently, we have paid special attention to the study of the photocurrent–time dependence associated with water photoelectrolysis at n-$TiO_2$ single crystals.[1f,t,u] In contrast to the flash photolysis technique, which employs very short light pulses (from picoseconds to nanoseconds), in our case the system was perturbed by long pulses produced with a mechanical shutter ($\approx$2 ms aperture speed) placed between a continuous illumination source and the PEC. This means that kinetic information about photoelectrochemical processes is restricted to a time scale in the range from milliseconds to seconds.

The main transient features of water splitting at $TiO_2$ photoelectrodes have been rationalized on the basis of a kinetic model involving two parallel mechanisms: (1) at low band-bending, a cathodic back reaction of valence band holes, trapped at photogenerated surface intermediates (mainly $OH^\circ_s$ and $(H_2O_2)_s$ peroxo species), with conduction band electrons; (2) a band-bending modulation associated with surface accumulation of positive charge (holes) at $OH^\circ_s$ species, having special incidence on the transients at high band-bending.[1f]

In the second case, the transient time constant, $\tau$, was found to be controlled by the $k_2$ rate constant of generation of surface peroxo species from the reaction between $OH^\circ_s$ radicals ($OH^\circ_s + OH^\circ_s \xrightarrow{k_2} (H_2O_2)_s$). $\tau$ was also found to decrease on increasing the density of donor centers $N_D$, which was attributed to the increase of $k_2$ with the concentration of oxygen vacancies generated during the $TiO_2$ reduction process in $H_2$ atmosphere.[1t] These findings seem to be consistent with the idea that $Ti^{3+}$–$V_O$–$T^{3+}$ lattice defects, where $V_O$ represents an oxygen vacancy generated by $TiO_2$ reduction (n-type doping process), behave as catalytic active centers in water photooxidation.

With this idea in mind, and in order to find out the influence of $N_D$ on the catalytic activity of $TiO_2$ electrodes in the photoassisted oxidation of water, we present here a detailed analysis of the photocurrent transient behavior obtained with a n-$TiO_2$ (001) rutile single crystal in contact with an indifferent aqueous electrolyte (pH 13), as a function of the concentration of $Ti^{3+}$ donor centers, ($Ti^{3+} \rightarrow Ti^{4+} + e^-_{CB}$) generated during $TiO_2$ reduction in $H_2$ atmosphere.

## Experimental Section

A n-$TiO_2$ (rutile) single crystal 10 × 10 mm and 1 mm thick was used. The (001) face exposed to the electrolyte was mechanically polished to a mirror finish with 0.3 $\mu$m $Al_2O_3$ and ultrasonically cleaned in dilute KOH and chemically etched in $H_2SO_4$ at 400 °C for 1 h, in order to remove the surface disturbed zone generated by polishing.[2] The crystal was then successively reduced in $H_2$ atmosphere according to the following heating treatments: (a) 400 °C for 30 min, (b) 500 °C for 30 min, and (c) 600 °C for 30 min. Consecutive photoelectrochemical experiments were performed after each treatment. The reduced rutile sample was mounted in a Teflon holder, which allows the ohmic In/Ga eutectic contact on the nonexposed face to be isolated of the electrolyte without using any cement. In this way, the $TiO_2$ photoelectrode can be easily dismounted for successive heating treatments and mounted again. The $TiO_2$ geometric area exposed was $\approx$0.38 cm$^2$. A conventional three-electrode configuration, flat-bottomed PEC built of Pyrex glass, with a quartz window, was used. It consisted of the photoelectrode, a high-area Pt counterelectrode, and a reference saturated calomel electrode (SCE) placed a few millimeters away from the photoelectrode. The electrolyte was a 0.1 M KOH aqueous solution made with Milli-Q ultrapure water and reagent grade chemicals (Merck). The photoelectrode was illuminated, through the quartz window, with a 150-W Xe lamp followed by an Oriel monochromator and neutral filters. The monochromatic photon flux, $\Phi_0$, absorbed by the electrode was measured with an IL 7000 A radiometer (International Light). Reflection losses at the cell window and at the electrode surface were assumed to be of the order of 10%. Photocurrent transients were obtained by $TiO_2$ photoexcitation with light pulses of several seconds duration. A mechanical shutter connected to the trigger of a digital oscilloscope (Trio, MS-1650 A) was used with this purpose. Experimental details of the photocurrent transient technique have been given elsewhere.[1f] The time resolution of the system ($\approx$2 ms), which is determined by the aperture speed of the shutter, was, in any case, greater than the RC time constant of the PEC. Transient time constants lower than $\approx$5 ms were never taken into consideration. Possible transient effects associated with the electroreduction of photogenerated $O_2$[1g] and/or local pH changes[1t] were eliminated by bubbling the electrolyte with $N_2$ under strong magnetic stirring. Semiconductor capacitances ($C_{sc}$) were obtained from measurements of impedance and phase angle, according to Tomkiewicz's method,[3] by using a lock-in amplifier (EG&G, PAR-5209) and a low-distortion audio generator (Leader, LAG-125). Potentiodynamic and potentiostatic measurements, both in the dark and under electrode illumination, were performed with a potentiostat (Wenking POS-73) connected to a fast X–Y recorder (YEW-303313).

0022-3654/92/2096-10349$03.00/0 

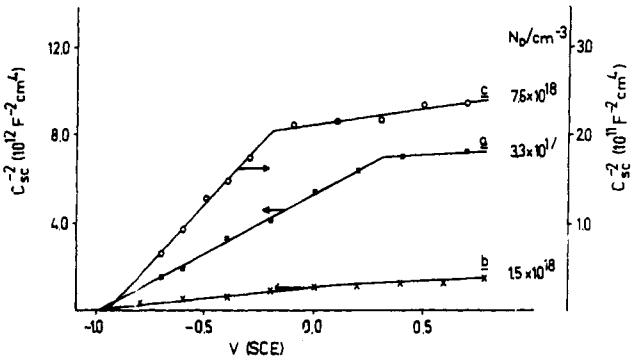


**Figure 1.** Mott–Schottky plots of the (001) n-$TiO_2$ rutile single crystal in 0.1 M KOH, after successive reduction treatments in $H_2$ atmosphere for 30 min, at (a) 400 °C, (b) 500 °C, (c) 600 °C.

## Results and Discussion

**Mott–Schottky Plots.** Mott–Schottky plots obtained after the three consecutive heating treatments in $H_2$ described in the Experimental Section are shown in Figure 1. The frequency used was 5 kHz, which is the maximum value admitted by our experimental device. A change of slope at variable potential can be observed in all the three cases and attributed to a nonuniform distribution of donor centers.[2] The fact that the slope of the segment at lower potentials increased when the electrode was chemically etched (oxidized) after the reduction treatments seems to confirm this hypothesis. According to Butler,[4] ionized donor centers diffuse from the bulk toward the electrode surface during $TiO_2$ reduction in $H_2$ atmosphere. This migration produces a surface layer, $10^2$–$10^3$-Å thick in our case, with a donor concentration ($N_D$) lower than that of the bulk. Although in both regions the slope is observed to increase slightly with the frequency, the intersection with the potential axis of the segment of high slope, which represents a measurement of the flatband potential ($V_{fb}$), was found to be frequency independent. $N_D$ was calculated from the well known Mott–Schottky expression

$$C_{sc}^{-2} = \frac{2}{\epsilon\epsilon_0 q N_D A^2}(V - V_{fb} - KT/q) \qquad (1)$$

where $\epsilon$ and $\epsilon_0$ are the semiconductor dielectric constant and the vacuum permitivity, respectively, $A$ is the actual electrode area exposed to the electrolyte, and the other symbols have their usual meaning. $N_D$ values calculated from the segments of high slope, corresponding to the near-surface region, are included in Figure 1. Taking into account that the slope of $C_{sc}^{-2}$ vs $V$ was found to increase with frequency, actual $N_D$ values are probably smaller than those obtained from Figure 1. The segments of low slope were not taken into consideration since only those photons absorbed in the near-surface region contribute to the photocurrent.

**Photocurrent Transients in the High Band-Bending Region.** When the $TiO_2$ photoelectrode is suddenly illuminated under potentiostatic conditions a transient photocurrent effect is generally observed.[1f] The inset of Figure 2 shows a typical photocurrent transient obtained at high band-bending. The initial photocurrent $I_{ph}(in)$ represents the separation of photogenerated electron–hole pairs and, therefore, is a measurement of the instantaneous flux of holes from the bulk toward the interface with the electrolyte, just when illumination starts ($t = 0$). Immediately, a slow photocurrent decay with time is observed, until a steady-state value $I_{ph}(st)$ is reached for $t \to \infty$. This effect has been attributed to a band-bending decrease associated with surface accumulation of holes at $OH^{\bullet}_s$ radicals.[1f] The lack of conduction band electrons at the surface at high band-bending hinder electron–hole recombination when the light is switched off and, therefore, the presence of a cathodic transient (cathodic back reaction).[1f] A plot of $I_{ph}(in)$ vs band-bending ($\phi_s$), for the (001) rutile single crystal in 0.1 M KOH after the successive reducing treatments (different values of $N_D$), under constant monochromatic illumination ($\Phi_0 \approx 1.1 \times 10^{15}$ cm$^{-2}$ s$^{-1}$ for $\lambda = 385$ nm), is also shown in Figure 2. The observed increase of $I_{ph}(in)$ with $N_D$ indicates an increasing strength of the electric field at the semiconductor space charge layer, producing a more efficient electron–hole separation.[5]

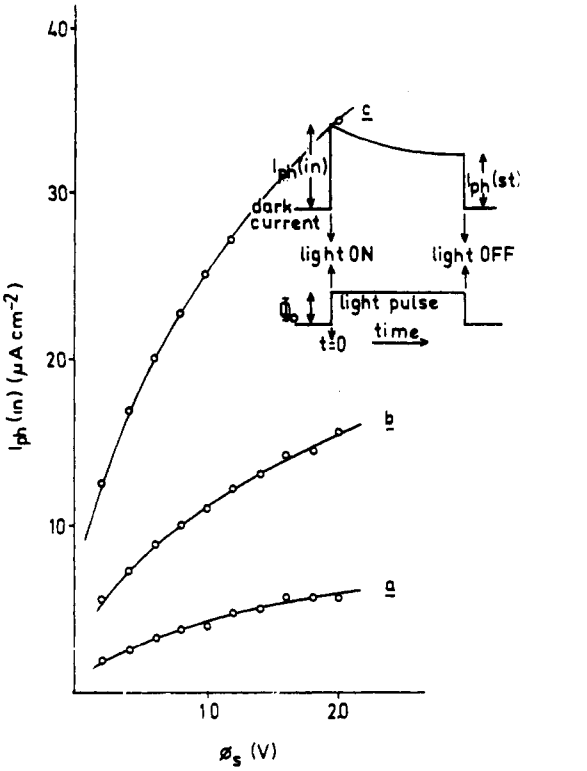


**Figure 2.** Plots of the initial photocurrent ($I_{ph}(in)$) vs band-bending ($\phi_s$) for the (001) rutile single crystal in 0.1 M KOH, after the same reduction treatments indicated in Figure 1. (Illumination conditions: $\lambda = 385$ nm, $\Phi_0 \approx 10^{15}$ cm$^{-2}$ s$^{-1}$). The inset shows a typical photocurrent transient at high band-bending ($\phi_s > 1$ V) under a quadratic light pulse of several seconds duration obtained with a mechanical shutter.

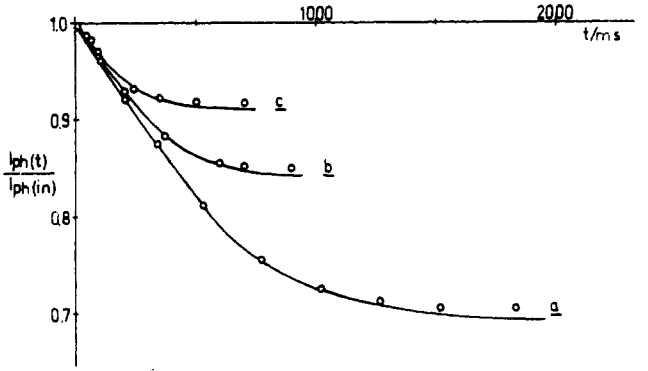


**Figure 3.** Normalized photocurrent transients for the (001) rutile single crystal in 0.1 M KOH, under monochromatic illumination ($\lambda = 385$ nm), after the reduction treatments indicated in Figure 1. The illumination intensity was controlled in order to maintain an $I_{ph}(in) \approx 16$ $\mu$A cm$^{-2}$ in all the three cases ($\phi_s \approx 1$ V). Solid lines represent the best theoretical fitting obtained through eq 17 by solving the system of differential equations (11)–(13). Boundary conditions and best fitting parameters are given in Table II.

The influence of $N_D$ on the relative photocurrent–time dependence is shown in Figure 3, where $I_{ph}(t)$ represents the photocurrent at any instant $t$ after illumination starts. In these experiments, the illumination intensity was controlled in order to maintain a constant flux or photogenerated holes toward the semiconductor–electrolyte interface (i.e., a constant $I_{ph}(in)$). It is worth noting that both the photocurrent decay and the time needed to reach the steady state diminish as $N_D$ increases.

**Kinetic Approach.** On the basis of different experimental observations during the past years, a model for the photooxidation of water at n-$TiO_2$ electrodes has been proposed.[1f,t,u] At basic pH, under high band-bending conditions where the conduction band at the $TiO_2$ surface is depleted of electrons and recombination

is hindered, oxygen evolution is the result of the following sequence of reaction steps:

$$TiO_2 + h\nu \xrightarrow{v_0} h^+_{VB} + e^-_{CB} \quad (2)$$

$$OH^-_s + h^+_{VB} \xrightarrow{v_1} OH^\circ_s \quad (3)$$

$$OH^\circ_s + OH^\circ_s \xrightarrow{v_2} (H_2O_2)_s + V_{OH^-_s} \quad (4)$$

$$(H_2O_2)_s + 2h^+_{VB} \xrightarrow{v_3} O_2\uparrow + 2H^+ + V_{OH^-_s} \quad (5)$$

$$V_{OH^-_s} + OH^-_{aq} \xrightarrow{v_4} OH^-_s \quad (6)$$

Reaction 2 takes into account $TiO_2$ absorption of photons and generation of photoelectrochemically active electron–hole pairs. According to (3), valence band photogenerated holes ($h^+_{VB}$) migrate toward the interface with the electrolyte where are trapped by chemisorbed $OH^-_s$ ions, giving rise to $OH^\circ_s$ radicals. Further, $OH^\circ_s$ species react on the $TiO_2$ surface according to (4), generating peroxo complexes (i.e., chemisorbed $H_2O_2$ molecules). Oxygen is finally evolved according to (5) via $h^+_{VB}$ oxidation of $(H_2O_2)_s$ molecules. $OH^-_s$ vacancies ($V_{OH}$) generated in steps 4 and 5 are filled with $OH^-_{aq}$ electrolyte ions at a very high rate, $v_4$. The rates of the main reaction steps can be written:

$$v_0 = \eta\Phi_0 \quad (7)$$

$$v_1 = k_1[h^+_{VB}]_s[OH^-_s] \quad (8)$$

$$v_2 = k_2[OH^\circ_s]^2 \quad (9)$$

$$v_3 = k_3[h^+_{VB}]_s[(H_2O_2)_s] \quad (10)$$

where $\Phi_0$ is the flux of absorbed photons and $\eta$ the quantum efficiency ($\eta = I_{ph}/q\Phi_0$).

The time dependence of $[OH^-_s]$, $[OH^\circ_s]$, and $[(H_2O_2)_s]$ concentrations can be obtained by solving the following system of differential equations:

$$d[OH^-_s]/dt = -v_1 + v_4 \quad (11)$$

$$d[OH^\circ_s]/dt = v_1 + 2v_2 \quad (12)$$

$$d[(H_2O_2)_s]/dt = v_2 - v_3 \quad (13)$$

**Photocurrent–Time Dependence Simulation.** The photocurrent transients at high band-bending can be simulated by means of the following expression[1f]

$$I_{ph}(t) = I_{ph}(in) - \Delta I_{ph}(t) \quad (14)$$

where $\Delta I_{ph}(t)$ represents the photocurrent diminution due to a band-bending decrease associated with the surface accumulation of holes (positive charge) in reaction 3. The contribution to $\Delta I_{ph}(t)$ of the band-bending modulation due to local pH changes is considered to be negligible at pH 13.[1i] Therefore, under our experimental conditions we can write

$$I_{ph}(t) = \frac{dI_{ph}(in)}{d\phi_s}\Delta\phi_s(t) \quad (15)$$

where

$$\Delta\phi_s(t) = \frac{\Delta Q_s(t)}{C_H} \equiv \frac{q[OH^\circ_s](t)}{C_H} \quad (16)$$

being $C_H \approx 20\ \mu F\ cm^{-2}$ the $TiO_2$ Helmholtz layer capacitance and $q$ the electron charge. The term $dI_{ph}(in)/d\phi_s$ in (15) represents the slope of $I_{ph}(in)$ vs $\phi_s$ curves of Figure 2.

By substituting (15) and (16) into (14) we obtain finally

$$I_{ph}(t) = I_{ph}(in) - \frac{dI_{ph}(in)}{d\phi_s}\frac{q[OH^\circ_s](t)}{C_H} \quad (17)$$

In order to be able to calculate $dI_{ph}(in)/d\phi_s$ in eq 17, the experimental curves of Figure 2 were fitted by means a fourth-order polynomial:

$$I_{ph}(in) = a\phi_s^4 + b\phi_s^3 + c\phi_s^2 + d\phi_s + e \quad (18)$$

The best fitting parameters $a$, $b$, $c$, $d$, and $e$ are given in Table I. $[OH^\circ_s](t)$ concentrations were obtained by solving the system of differential equations (11)–(13) by GEAR[6] and GIT[7] computer methods. The solid lines of Figure 3 show the best fitting of eq 17 to experimental transients. The following initial conditions were used: $[OH^-_s]_{in} = 10^{-15}\ cm^{-2}$, which corresponds to a reasonable $OH^-$ surface coverage near one monolayer, and $[OH^\circ_s]_{in} = [(H_2O_2)_s]_{in} = [V_{OH}]_{in} = 0$. Under these conditions the fitting was found to be mainly determined by the $k_2$ rate constant for $OH^\circ_s$ reaction. The best fitting parameters are given in Table II. The fact that $k_3 \gg k_1$ seems to indicate that the cross section for hole capture is considerable greater for photogenerated $(H_2O_2)_5$ species than for chemisorbed $OH^-$ ions.

**The Catalytic Role of Oxygen Vacancies.** A plot of the best fitting $k_2$ values vs $N_D$ is shown in Figure 4. The linear increase of $k_2$ (the rate constant for surface $OH^\circ_s$ combination) with $N_D$ suggests a catalytic activation of the rutile surface during the reduction treatment.

It is well-known that donor centers generated by $TiO_2$ reduction in $H_2$ atmosphere are associated with lattice defects of the type $2Ti^{3+}$–$V_O$, where $V_O$ represents an oxygen vacancy.[8] These defects

**TABLE I: Best Fitting Parameters of Eq 18 to Experimental Curves of Figure 2**

| | a | b | c | d | e |
|---|---|---|---|---|---|
| curve a | −1.22 | 5.96 | −10.48 | 9.71 | 0.22 |
| curve b | −3.05 | 14.95 | −26.39 | 24.56 | 1.15 |
| curve c | −8.11 | 39.7 | −69.50 | 62.80 | 3.31 |

**TABLE II: Parameters Used To Solve the System of Time-Dependent Differential Equations 11–13, in Order To Fit Experimental Data of Figure 3 through Eq 17[a]**

| | $K_1$ ($cm^2\ s^{-1}$) | $K_2$ ($cm^2\ s^{-1}$) | $K_3$ ($cm^2\ s^{-1}$) |
|---|---|---|---|
| curve a | $3.7 \times 10^{-12}$ | $7.2 \times 10^{-15}$ | $3.4 \times 10^{-10}$ |
| curve b | $1.2 \times 10^{-12}$ | $2.4 \times 10^{-14}$ | $1.4 \times 10^{-10}$ |
| curve c | $1.4 \times 10^{-12}$ | $8.5 \times 10^{-14}$ | $1.4 \times 10^{-10}$ |

[a] Initial conditions: $[OH^-_s]_{in} = 10^{-15}\ cm^{-2}$; $[OH^\circ_s]_{in} = [(H_2O_2)_s]_{in} = [V_{OH_s}^-]_{in} = 0$.

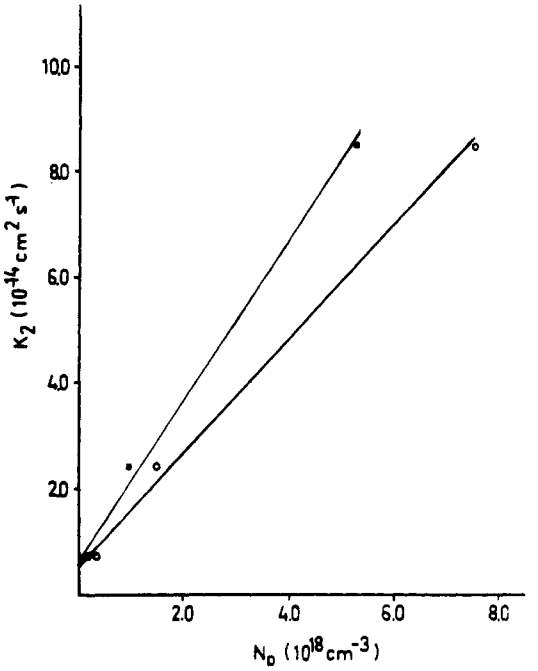


**Figure 4.** Plot of the calculated $k_2$ rate constant vs $N_D$ values obtained from (○) Mott–Schottky plots of Figure 1; (■) $\eta$ vs $\phi_s^{1/2}$ plots of Figure 6.

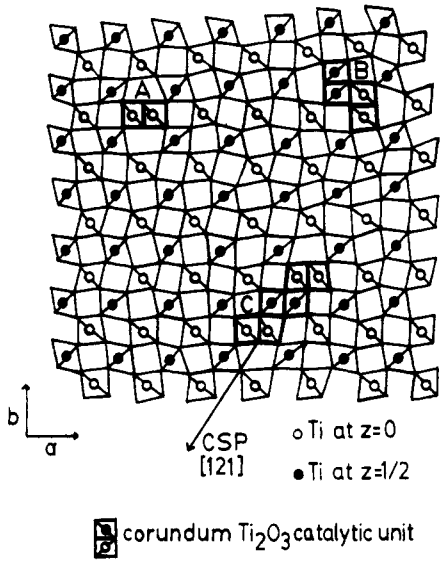


**Figure 5.** Idealized rutile [001] bounded projection according to Bursill et al.,[13] showing aggregation of $Ti_2O_3$ corundum units generated from the annihilation of oxygen vacancies and the simultaneous lattice reconstruction. A small linear defect is shown in (A). Addition of similar units in (B) and (C) leads to an incipient CS plane along [121].

are not only responsible for the n-type conductivity of $TiO_2$, something well established, but also for its catalytic activity in water photooxidation, as we try to show here. In fact, there is indirect spectroscopic evidence that $Ti^{3+}$ ions behave as active centers for water splitting at n-$TiO_2$,[9] although the origin of $Ti^{3+}$ catalytic activity is not well-known. As we have suggested previously,[10] the catalytic role of $2Ti^{3+}$–$V_O$ defects (formally $Ti_2O_3$ units) may be connected with the short distance between $Ti^{3+}$ pairs, which makes easy the surface reaction of $OH^\circ_s$ radicals associated with them (i.e., reduces the activation energy for reaction 4).

At very low concentrations, oxygen vacancies are believed to be randomly distributed in the $TiO_2$ lattice as point defects. Nevertheless, as $[V_O]$ increases a clear tendency seems to exist for these defects to become ordered, it being accepted that for large enough departures from stoichiometry (i.e., for sufficiently high $N_D$ values) oxygen vacancies rearrange, giving rise to microdomains known as crystallographic shear (CS) planes.[11] There is some controversy about the critical value of $\delta$ for which $Ti_2O_3$ point defects in reduced rutile ($TiO_{2-\delta}$) rearrange at CS planes. For instance, according to Tilley et al.,[12] CS extended defects are one of the most stable in the slightly reduced $TiO_2$ rutile, even in the reduction range where interstitial Ti ions are regarded as the dominant point defects. Therefore, reduced $TiO_2$ (i.e., $TiO_{2-\delta}$) for all but infinitesimal $\delta$ values (e.g., $\delta = 10^{-5}$ for $N_D \approx 10^{18}$ cm$^{-3}$) would consist largely of $Ti_2O_3$ corundum microdomains coherent with the rutile structure.[11,12] An idealized (001) projection of $[TiO_6]$ octahedral arrangement in rutile, including different states of aggregation of $Ti_2O_3$ units is shown in Figure 5. It is evident from this figure the drastic shortening of the $Ti^{3+}$–$Ti^{3+}$ distance in $Ti_2O_3$ corundum units (2.59 Å) with respect to the corresponding $Ti^{4+}$–$Ti^{4+}$ between neighbors $[TiO_6]$ octahedra in rutile nondefective regions (4.59 Å). In consequence, $Ti_2O_3$ detects, no matter where they are ordered (CS planes) or randomly distributed (point defects), should behave as catalytic units where the probability of reaction between $Ti^{3+}$ adsorbed $OH^\circ_s$ radicals drastically increases. This assumption is sustained by recent Harding's theoretical calculations on the $H_2O_2$ potential surface,[14] according to which the interaction energy between two $OH^\circ$ radicals has a well-defined potential barrier with a maximum at ≈3.0 Å. For O–O distances larger than 3.0 Å, the potential energy of $H_2O_2$ species is dominated by a repulsive dipole–dipole interaction between $OH^\circ_s$ radicals, while at the other side of the barrier (i.e., for O–O distances smaller than 3.0 Å), the energy wave function switches to a strong covalent bonding. It seems, therefore, reasonable to assume that surface generation of $(H_2O_2)_s$ species from photogenerated $OH^\circ_s$ radicals should be dramatically enhanced at $Ti_2O_3$ corundum units, as the separation between $OH^\circ_s$ radicals attached to adjacent $Ti^{3+}$ ions (2.59 Å) is below the critical distance for covalent bonding obtained by Harding. In contrast, outside $Ti_2O_3$ catalytic units (i.e., in nondefective rutile regions) $H_2O_2$ formation from adsorbed $OH^\circ_s$ species should be hindered, as the $Ti^{4+}$–$Ti^{4+}$ distance is 4.59 Å. However, because of the weak interaction of the $OH^\circ_s$ radicals with the semiconducting substrate, their thermal mobility on the $TiO_2$ surface may be high enough as to promote formation of covalent bonding between $Ti^{4+}$ adsorbed $OH^\circ$ species, although the $OH^\circ_s$ reaction rate should be much smaller to than at corundum catalytic units. Approximately 1 kcal/mol is the repulsive dipole–dipole interaction energy to be overcome for $OH^\circ$ radicals to become covalent bonded.[14]

Consequently, two regions with different catalytic activity could be distinguished at the (001) face of our $TiO_{2-\delta}$ rutile single crystal: (1) those $Ti_2O_3$ corundum units, characterized by a high rate constant for $OH^\circ_s$ reaction, $k'_2$; (2) nondefective rutile regions with a much smaller $k''_2$ rate constant. In a first approximation, we can assume that the experimental value of $k_2$ is given by the expression

$$k_2 = k'_2\Theta + k''_2(1 - \Theta) \tag{19}$$

where $\Theta$ is the fraction of rutile surface occupied by $Ti_2O_3$ units.

Considering that the rutile unit cell contains 4 oxygens in a volume of 62.4 Å$^3$, the maximum possible concentration of oxygen vacancies, which correspond to a total conversion of $TiO_2$ into $Ti_2O_3$, is $6.4 \times 10^{22}$ cm$^{-3}$; but $[V_O] = N_D/2$ and, therefore, we can write

$$\Theta \approx N_D/3.2 \times 10^{22} \tag{20}$$

so that eq 19 becomes

$$k_2 = k''_2 + [(k'_2 - k''_2)/3.2 \times 10^{22}]N_D \tag{21}$$

According to eq 21, the plot of $k_2$ vs $N_D$ should be linear, as it is experimentally observed in Figure 4, with a slope $(k'_2 - k''_2)/3.2 \times 10^{22}$ and an intercept with the vertical axis $k''_2$. Therefore, by applying eq 21 to the data of Figure 4, for $N_D$ values obtained from Mott–Schottky plots (Figure 1) we have $k'_2 = 5.9 \times 10^{-10}$ cm$^2$ s$^{-1}$ and $k''_2 = 7 \times 10^{-15}$ cm$^2$ s$^1$. Because of the relatively low frequency used to obtain Mott–Schottky plots (5 kHz), $N_D$ values obtained from Figure 1 are probably calculated in excess. In order to obtain more precise $N_D$ values, photocurrent measurements were used. In fact, by application of Gärtner's model to the semiconductor–electrolyte junction the following simplified expression for the PEC photocurrent is obtained[5]

$$I_{ph} = q\Phi_0\left(1 - \frac{e^{-\alpha W}}{1 + \alpha L_p}\right) \tag{22}$$

where $\alpha$ is the absorption coefficient for incident photons, $W$ the depletion layer width and $L_p$ the hole diffusion length in the absence of electric field. For the case that $\alpha W \ll 1$, we have shown that[2]

$$\eta \equiv I_{ph}/q\Phi_0 = Q\alpha L_p + Q\alpha W = Q\alpha L_p + [\alpha(q/\epsilon\epsilon_0)^{1/2}N_D^{1/2}(L'^2_p q/KT)]\phi_s^{1/2} \tag{23}$$

where the "gain factor"

$$Q = L'^2_p q^2 N_D/2\epsilon\epsilon_0 KT \tag{24}$$

takes into account the efficiency for separation of $h^+_{VB}$–$e^-_{CB}$ pairs within the electric field region (i.e., for small enough $N_D$, $Q < 1$ and recombination takes place at the space charge layer) and $L'_p$ is the hole diffusion length within the depletion layer.

For (001) n-$TiO_2$ rutile, $Q < 1$ if $N_D \leq 6 \times 10^{18}$ cm$^{-3}$,[2] so that eq 23 should apply to our experimental data. In fact, Figure 6 shows a linear plot of $\eta$ vs $\phi_s^{1/2}$ from experimental data of Figure 2. The $N_D$ values calculated from the different slopes of Figure 6, for $\epsilon = 180$, $\alpha = 2 \times 10^4$ cm$^{-1}$ and $L'_p = 9 \times 10^{-7}$ cm,[2] are slightly smaller than those obtained from capacitance measurements. The linear correlation between $k_2$ and the new values of $N_D$ are also shown in Figure 4. In this case the intercept with

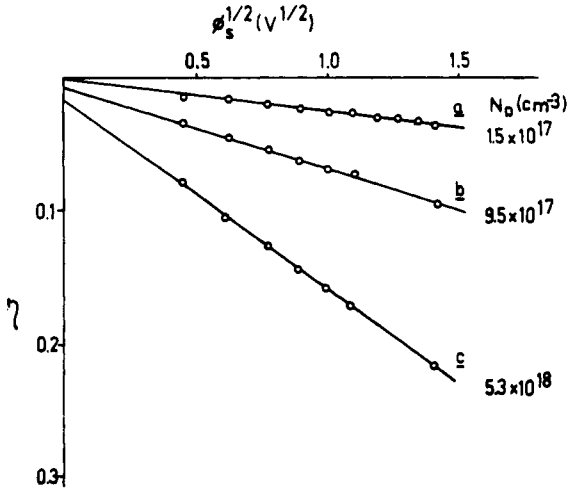


**Figure 6.** Photocurrent quantum efficiency ($\eta$) vs $\phi_s^{1/2}$ plots obtained from the experimental data of Figure 2.

the vertical axis gives us a $k''_2 = 5.0 \times 10^{-15}$ and the slope a $k'_2 = 5.0 \times 10^{-10}$ cm$^2$ s$^{-1}$, very close to $k'_2$ and $k''_2$ values associated with $N_D$ values obtained from Mott-Schottky plots.

As far as eq 19 and 20 are valid, these results shows that the catalytic activity of $Ti_2O_3$ corundum units associated with oxygen vacancies is characterized by a rate constant for $OH^\circ_s$ reaction about 5 orders of magnitude greater than that the characterizing rutile regions free of this kind of lattice defect.

## Conclusions

We have shown that the time decay characterizing the photocurrent transients observed during water photoelectrolysis at (001) n-$TiO_2$ rutile in basic medium, and in the absence of surface recombination (high enough band-bending) is very sensitive to the concentration of donor centers $N_D$. Under these conditions, the photocurrent-time dependence is due to the surface accumulation of positive holes, the photocurrent-time decay being controlled by rate of generation of $(H_2O_2)_s$ species from the surface reaction between photogenerated $OH^\circ_s$ radicals.[1u] The experimental observation that the rate constant for $(H_2O_2)_s$ generation, $k_2$, increases linearly with $N_D$ suggests that $Ti^{3+}$-$V_O$-$Ti^{3+}$ lattice defects generated by $TiO_2$ reduction in $H_2$ atmosphere behave as active centers for the photoassisted oxidation of $H_2O$ to $H_2O_2$ on the semiconductor surface. The catalytic properties of $Ti_2O_3$ corundum units are attributed to the short distance between adjacent $Ti^{3+}$ ions (2.59 Å), which is considerably smaller than the corresponding $Ti^{4+}$-$Ti^{4+}$ distance in the nondefective rutile regions (4.59 Å). This assumption is supported by recent calculations of Harding, according to which for O-O separations lower than ≈3.0 Å the covalent bonding involved in the formation of $H_2O_2$ peroxo species is found to be the dominant attractive force between two interacting $OH^\circ$ radicals.

*Acknowledgment.* This work was supported by the CICyT, Spain (Project MAT 89-0862-C03-01).

**Registry No.** $TiO_2$ rutile, 1317-80-2; $H_2O_2$, 7722-84-1; $Ti_2O_3$, 1344-54-3; $Ti^{3+}$, 22541-75-9; water, 7732-18-5.

## References and Notes

(1) (a) Rajeshwar, K. *J. Electrochem. Soc.* **1982**, *129*, 1003. (b) Pajkossy, T. *J. Electrochem. Soc.* **1983**, *130*, 632. (c) Abrantes, L. M.; Peter, L. M. *J. Electronal. Chem.* **1983**, *150*, 593. (d) Peter, L. M.; Li, J.; Peat, R. *J. Electronal. Chem.* **1984**, *165*, 29. (e) Li, J.; Peat, R.; Peter, L. M. *J. Electronal. Chem.* **1984**, *165*, 41. (f) Salvador, P. *J. Phys. Chem.* **1985**, *89*, 3863. (g) Tafalla, D.; Salvador, P. *J. Electroanal. Chem.* **1987**, *237*, 255. (h) Sagara, T.; Sukigara, M. *J. Electrochem. Soc.* **1988**, *135*, 363. (i) Albery, W. J.; Dias, N. L.; Wilde, C. P. *J. Electrochem. Soc.* **1987**, *134*, 601. (j) Deutscher, S. B.; Richardson, J. H.; Perone, S. P.; Rosenthal, J.; Ziemer, J. N. *Faraday Discuss. Chem. Soc.* **1980**, *70*, 35. (k) Perone, S. P.; Richardson, J. H.; Deustcher, S. B.; Rosenthal, J.; Ziemer, J. N. *J. Electrochem. Soc.* **1980**, *127*, 2580. (l) Kamat, P. V.; Fox, M. A. *J. Phys. Chem.* **1983**, *87*, 59. (m) Hartig, J. J.; Grabner, G.; Getoff, N.; Popkirov, G.; St. Kanev, G. *Ber. Bunsenges. Phys. Chem.* **1985**, *89*, 831. (n) Norton, A. P.; Bernasek, S. L.; Bocarsly, A. B. *J. Chem. Phys.* **1988**, *92*, 6009. (p) Harzinou, Z.; Coroiture, N.; Gottesfeld, S. *J. Electrochem. Soc.* **1981**, *128*, 551. (q) Wilson, R. H.; Sakata, T.; Kawai, T.; Hasimoto, K. *J. Electrochem. Soc.* **1985**, *132*, 1082. (r) Neumann-Spallart, M.; Schwartz, A.; Grabner, G. *J. Phys. Chem.* **1984**, *93*, 1984. (s) Sakata, T.; Janata, E.; Jaegermann, W.; Tributsch, H. *J. Electrochem. Soc.* **1986**, *133*, 339. (t) Tafalla, D.; Salvador, P. *J. Electroanal. Chem.* **1989**, *270*, 285. (u) Tafalla, D.; Salvador, P.; Benito, R. M. *J. Electrochem. Soc.* **1990**, *310*, 810.
(2) Salvador, P. *J. Appl. Phys.* **1984**, *55*, 2977.
(3) Tomkiewicz, M. *J. Electrochem. Soc.* **1979**, *126*, 221.
(4) Butler, M. A. *J. Electrochem. Soc.* **1979**, *126*, 339.
(5) Gärtner, W. W. *Phys. Rev.* **1959**, *116*, 84.
(6) Stabler, R. N.; Chesick, J. P. *Int. J. Chem. Kinet.* **1978**, *10*, 461. McKinney, J.; Weigert, F. J., private communication.
(7) Weigert, F. J. *Comput. Chem.* **1987**, *11*, 273.
(8) Göpel, W.; Rocker, G.; Feirabend, R. *Phys. Rev. B* **1983**, *28*, 3427.
(9) Lo, W. J.; Chang, Y. W.; Somorjai, G. A. *Surf. Sci.* **1978**, *71*, 199.
(10) Salvador, P. *New J. Chem.* **1988**, *12*, 35.
(11) Anderson, J. S.; Hyde, B. G. *J. Phys. Chem. Solids* **1967**, *28*, 1393.
(12) Sawatari, H.; Iguchi, E.; Tilley, R. D. *J. Phys. Chem. Solids* **1982**, *43*, 1147.
(13) Smith, D. J.; Bursill, L. A.; Blanchin, M. G. *Philos. Mag. A* **1984**, *50*, 473.
(14) Harding, L. B. *J. Phys. Chem.* **1991**, *95*, 8653.

# CO Hydrogenation on $Cr_2O_3$-Promoted Copper Catalysts

**Hsiu-Wei Chen* and Jarrn-Horng Lin**

*Department of Chemistry, National Sun Yat-Sen University, Kaohsiung, Taiwan, Republic of China*
*(Received: March 18, 1992)*

The promotion effect of $Cr_2O_3$ on copper catalysts has been studied on $Cu/Cr_2O_3$, $Cu/Cr/SiO_2$, and $Cu/SiO_2$ catalysts. CO hydrogenation reaction was applied as a probe to test the activity of the catalysts. The activities of $Cu/Cr_2O_3$ catalysts for CO hydrogenation are highly dependent on the variations of the particle size of the supported copper and the temperature of reduction treatments. $Cu/Cr/SiO_2$ catalysts have similar behavior as the $Cu/Cr_2O_3$ catalysts. $SiO_2$-supported copper catalysts are insensitive to the change of pretreatment conditions of the catalysts and the amounts of copper loading on the support. The origin of the promotion ability of $Cr_2O_3$ on copper catalysts was discussed on the basis of an electronic interaction model.

## Introduction

Copper catalyst is one of the interesting catalyst systems that is strongly effected by the supports. Consider, for example, the CO hydrogenation activity of copper metal is much higher than that of bulk copper when $Cr_2O_3$ or ZnO is used as a support. When $SiO_2$ or $Al_2O_3$ is used as a support, the supported copper has about the same activity as bulk copper.[1-5] Several models have been proposed to explain these phenomena. The major concern of the models is about the active center of copper catalysts in hydrogenation reaction. They fall into three main categories:

0022-3654/92/2096-10353$03.00/0 